Impact of water uptake and mixing state on submicron particles deposition in the human respiratory tract (HRT): Based on explicit hygroscopicity measurements at HRT-like conditions

Ruiqi Man[1], Zhijun Wu[1,2], Taomou Zong[1], Aristeidis Voliotis[3,4], Yanting Qiu[1], Johannes Größ[5], Dominik van Pinxteren[5], Limin Zeng[1], Hartmut Herrmann[5], Alfred Wiedensohler[5], Min Hu[1]

[1]State Key Joint Laboratory of Environmental Simulation and Pollution Control, College of Environmental Sciences and Engineering, Peking University, 100871, Beijing, China

[2]Collaborative Innovation Center of Atmospheric Environment and Equipment Technology, Nanjing University of Information Science and Technology, 210044, Nanjing, China

[3]National Centre for Atmospheric Science, Department of Earth and Environmental Science, School of Natural Sciences, The University of Manchester, Oxford Road, M13 9PL, Manchester, UK

[4]Centre for Atmospheric Science, Department of Earth and Environmental Science, School of Natural Sciences, The University of Manchester, Oxford Road, M13 9PL, Manchester, UK

[5]Leibniz Institute for Tropospheric Research, 04318, Leipzig, Germany

Correspondence to: Zhijun Wu (zhijunwu@pku.edu.cn)

Abstract. The particle hygroscopicity plays a key role in determining the particle deposition in the human respiratory tract (HRT). In this study, the effects of hygroscopicity and mixing state on regional and total deposition doses based on the particle number concentration for the children, adults, and the elderly were quantified using the Multiple-Path Particle Dosimetry model based on the size-resolved particle hygroscopicity measurements at HRT-like conditions (relative humidity = 98%) performed in the North China Plain. The measured particle population with an external mixing state was dominated by hygroscopic particles (number fraction = (91.5 ± 5.7)%, mean ± standard deviation (SD), the same below). Particle hygroscopic growth in the HRT led to a reduction by around 24% in the total doses of submicron particles for all age groups. Such reduction was mainly caused by the growth of hygroscopic particles and was more pronounced in the pulmonary and tracheobronchial regions. Regardless of hygroscopicity, the elderly group had the highest total dose among the three age groups, while the children received the maximum total deposition rate. With 270 nm in diameter as the boundary, the total deposition doses of particles smaller than this diameter were overestimated and those of larger particles were underestimated assuming no particle hygroscopic growth in the HRT. From the perspective of the daily variation, the deposition rates of hygroscopic particles with an average of $(2.88 \pm 0.81) \times 10^9$ #/h during the daytime were larger than those $(2.32 \pm 0.81) \times 10^9$ #/h at night $((2.32 \pm 0.81) \times 10^9$ #/h). On the contrary, hydrophobic particles interpreted as freshly emitted soot and primary organic aerosols exhibited higher deposition rates at nighttime $((3.39 \pm 1.34) \times 10^8$ #/h) than those in the day $((2.58 \pm 0.76) \times 10^8$ #/h). The traffic emissions during the rush hours enhanced the deposition rate of hydrophobic particles. This work provides a more explicit assessment of the

37   impact of hygroscopicity and mixing state on the deposition pattern of submicron particles in the HRT.

38   **Keywords:** hygroscopicity; mixing state; HH-TDMA; lung deposition; MPPD

1 Introduction

Toxicological and epidemiological studies showed that ambient particles can result in the declining life expectancy and rising premature mortality (Chen et al., 2013; Correia et al., 2013; Pope and Dockery, 2013; Dockery et al., 1993; Pope et al., 2009). Compared with coarse particles, submicron particles (i.e., particles with diameter ≤ 1 μm) have smaller sizes and larger specific surface areas, which tend to carry more toxic and harmful components and reach deeper into the human respiratory tract (HRT) (Oberdorster, 2001). Inhaled particles deposit along the HRT mainly by diffusion, sedimentation, impaction, and interception (Wang et al., 2018a). The major deposition mechanism depends on the particle size and specific deposition location (Varghese and Gangamma, 2009). Unlike ambient environments, conditions in the HRT are warm and humid, where the relative humidity (RH) can be as high as 99.5% (Hussein et al., 2013). The unique environment can alter the chemical and physical characteristics of inhaled particles, leading to variations in particle deposition distributions and doses. To accurately quantify the deposition pattern of submicron particles in the HRT, it is therefore critical to account for such potential transformations and characterize inhaled particle properties in the HRT.

Due to experimental limitations of measuring inhaled particle number size distributions (PNSDs), regional doses in the HRT are typically estimated by means of mathematical models (Hofmann, 2011). The most widely used dosimetry models are the International Commission on Radiological Protection (ICRP, 1994) model and the Multiple-Path Particle Dosimetry (MPPD) model (Asgharian et al., 2001). Estimating the particle deposition fraction (DF) in these models is based on aerosol properties as well as individual's physiological parameters. These available dosimetry models, however, fail to incorporate some critical particle characteristics, especially the hygroscopicity (Ferron, 1977), which may cause variations in the particle size and therefore affect the deposition efficiency and pattern of particles in different lung regions.

To date, many studies have assessed the effects of hygroscopicity on ambient particle deposition in the HRT based on assumed values of the hygroscopic parameter (Kappa, κ) representing non-hygroscopic, nearly hydrophobic, and hygroscopic particles (Voliotis and Samara, 2018) or estimations ~~using~~ by parametric methods ~~models from κ of each chemical composition~~(Ching and Kajino, 2018; Hussein et al., 2013; Mitsakou et al., 2007; Haddrell et al., 2015; Vu et al., 2018). ~~(Chalvatzaki and Lazaridis, 2018; Ching and Kajino, 2018; Haddrell et al., 2015; Hussein et al., 2013; Martonen and Schroeter, 2003; Rajaraman et al., 2020; Vu et al., 2015; Vu et al., 2018; Xu et al., 2021; Londahl et al., 2007).~~ However, it is well-known that continental aerosols typically show an external mixing state and size-dependent hygroscopicity (Zong et al., 2021). Thus, in order to capture the real and high-time-resolution features of ambient particles' hygroscopic growth in the HRT, direct particle hygroscopic growth measurements are a matter of necessity.

To our best knowledge, there are only limited studies exploring the impact of the hygroscopic growth of ambient particles on the particle deposition by direct hygroscopicity measurements. Moreover, hygroscopicity measurements using the Humidity Tandem Differential Mobility Analyzer (H-TDMA) (Londahl et al., 2009; Farkas et al., 2022; Vu et al., 2015; Kristensson et al., 2013) or Differential Aerosol Sizing and Hygroscopicity Spectrometer Probe (DASH-SP) (Youn et al., 2016) in these studies were all

conducted at relatively lower RH (~ 90%) compared to that in the HRT (RH = 99.5%). ~~Hygroscopicity measurements of ambient aerosols under subsaturated conditions are mainly conducted by Humidity Tandem Differential Mobility Analyzer (H-TDMA) (Farkas et al., 2022; Kristensson et al., 2013; Londahl et al., 2009) or Differential Aerosol Sizing and Hygroscopicity Spectrometer Probe (DASH-SP) (Cuevas Robles et al., 2021; Youn et al., 2016).~~ For example, Farkas et al. (2022) modelled DFs of aerosol particles with four different diameters and studied in their dry state and after their hygroscopic growth at RH = 90% using a H-TDMA. Youn et al. (2016) examined size-resolved hygroscopicity data by DASH-SP for particles sampled near mining and smelting operations to study the effects of particles' hygroscopic growth on the HRT deposition of toxic contaminants. ~~Most of such studies used hygroscopicity data measured at considerably lower RH conditions opposed to those occurring in the HRT (85%-90% vs. ≈ 99.5%) (Vu et al., 2015; Swietlicki et al., 2008).~~ It was further assumed that κ was independent of RH on the premise that the effective molar volume of the solute does not vary with RH. However, the presence of surface active, slightly soluble substances, and the co-condensation of semi-volatile soluble organic compounds can result in the humidity-dependent characteristic of κ (Wu et al., 2013; Wex et al., 2009; Topping and Mcfiggans, 2012). For instance, Liu et al. (2018) showed that κ could vary from about 0.1 at RH < 20% to less than 0.05 when RH ≈ 90% due to the non-ideal mixing of water with hydrophobic and hydrophilic organic components. Therefore, an explicit hygroscopicity measurements at HRT-like conditions will make the deposition estimation more accurate.

In this study, the size-resolved particle hygroscopicity derived from a high humidity tandem differential mobility analyzer (HH-TDMA) at HRT-like conditions (RH = 98%) was first used to quantify the effects of both hygroscopicity and external mixing state on the particle deposition in the HRT using the MPPD model. The deposition doses of submicron particles were calculated in the head, tracheobronchial (TB), and pulmonary (P) regions in the HRT for different age groups. Further, the diurnal variations of deposition rates of hygroscopic and hydrophobic particles were also calculated to provide an insight into the particle deposition linked to human activities.

2 Materials and Methods

2.1 The Sampling Site and Instruments

The field campaign was conducted from June 8 to July 6 in 2014 at an ecological park in the rural area of Wangdu County (38.666ºN, 115.210ºE) in the North China Plain, a polluted area with high population density and strong primary emissions. The surroundings were wheat fields without significant industry emissions. A detailed description of the sampling site can be found in our previous study (Wu et al., 2017b). In brief, a HH-TDMA and a twin differential mobility particle sizer (TDMPS) were employed to measure the hygroscopic growth factor (HGF) of specific size particles at RH = 98% and the size-resolved PNSDs of particles ranging from 3 to 800 nm respectively. Besides, NO and CO was monitored by a NOx chemiluminescence analyzer (42i-TLE, Thermo Scientific) and a Trace Level Carbon Monoxide Analyzer

111 (48iQ, Thermo Scientific), respectively (Chen et al., 2020). The BC mass concentrations were measured by

112 a Multi-Angle Absorption Photometer (MAAP Model 5012, Thermo, Inc.) (Wang et al., 2019). The OH

113 radical was measured by a Laser-induced fluorescence (LIF) (Tan et al., 2020).

2.2 Particle Hygroscopic Growth Measurement

115 The HH-TDMA was designed to measure the aerosol hygroscopic growth at high RH (90% - 98%),

116 using the technique of a temperature-controlled water bath, which is able to hold the RH of aerosols and

117 sheath flow stable for RH > 90% (Hennig et al., 2005). The RH in the second differential mobility analyzers

118 (DMA) reached an absolute accuracy of ±1.2% for 98% and a long-term stability of ±0.1-0.4% of set point

119 values (Hennig et al., 2005). More detailed information regarding the HH-TDMA system was provided by

120 Bian et al. (2014) and Wu et al. (2017a). The HGF was defined as the ratio of the wet particle diameter at a

121 given RH ($D_{P,wet}$) to the dry particle diameter for RH < 10% ($D_{P,dry}$):

$$HGF = \frac{D_{P,wet}}{D_{P,dry}}, \tag{1}$$

122 The TDMAinv method developed by Gysel et al. (2009) was used to invert hygroscopicity data of settled

123 diameter particles (30, 50, 100, 150, 200, and 250 nm) to HGFs of size-resolved particles and hygroscopic

124 growth factor probability distribution function (GF-PDF) at RH = 98% (Gysel et al., 2009). The HGF was

125 then converted into the hygroscopic parameter (κ) according to the κ-Köhler theory (Petters and Kreidenweis,

126 2007):

$$\kappa = (HGF^3 - 1)(\frac{\exp\left(\frac{A}{D_{P,dry} \cdot HGF}\right)}{RH} - 1), \tag{2}$$

$$A = \frac{4\sigma_{s/a}M_w}{RT\rho_w}, \tag{3}$$

127 where HGF and $D_{P,dry}$ are the hygroscopic growth factor measured at 98% RH by HH-TDMA and the dry

128 particle diameter respectively. $\sigma_{s/a}$ is the droplet surface tension (assumed to be that of pure water, $\sigma_{s/a}$ =

129 0.0728 N m^{-2}). M_w is the molecular weight of water. ρ_w is the density of liquid water. R is the universal gas

130 constant, and T is the absolute temperature.

131 The head region, or upper respiratory tract, includes the nasal cavities, the pharynx, and the larynx. In

132 this study, the wet diameter of aerosols above the larynx was assumed to be equilibrated with ambient air

133 conditions (Ching and Kajino, 2018), therefore set to the average value during the sampling period (T = 26 ℃,

134 RH = 60%). The TB and P regions belong to the lower respiratory tract which were saturated with water

135 vapor, and the temperature and RH inside were 37 ℃ and 99.5%, respectively (Vu et al., 2015). The wet

136 particle diameter in the HRT was estimated by using the variant of Eq (2). Detailed information can be found

137 in Farkas et al. (2022). It should be noticed that the inhaled particle was assumed to reach the equilibrium

138 size immediately once particles enter into the HRT in this study. However, the hygroscopic growth rate of

139 particles depends on the particle size, hygroscopicity, the ambient environment conditions (such as RH and

140 temperature), and the residence time in the body (Ching and Kajino, 2018). A previous study pointed out that

141   particles with D_p = 100 nm can reach the equilibrium size in a few seconds, while the equilibrium timescale

142   of particles with D_p > 1 μm turn to minutes (Ching and Kajino, 2018).

2.3 Total, Hygroscopic, and Hydrophobic Particle Number Size Distributions

144   The TDMPS includes two Hauke-type DMA that have different effective center rod lengths which

145   measure aerosol particles of 20 - 800 nm and 3 - 20 nm, respectively. The two condensation particle counters

146   (CPC) count particles downstream of DMAs. Combining the counts from the two CPCs, the TDMPS can

147   measure the PNSD of particles from 3 to 800 nm (electrical mobility diameter). The instrument principle and

148   structure of TDMPS can be found in Birmili et al. (1999) and Wiedensohler et al. (2012). To match the

149   particle size range in the MPPD model, the electrical mobility diameter was converted to aerodynamic

150   diameter by Eq (4) (Khlystov et al., 2004):

$$d_a = d_m \sqrt{\mathcal{X} \times \frac{\rho \times C_{c(dm)}}{C_{c(da)}}}, \tag{4}$$

151   where d_a and d_m is the particle aerodynamic diameter (nm) and electrical mobility diameter (nm),

152   respectively. ρ is the particle density (1.5 g cm^{-3} in this study (Hu et al., 2012)). $\mathcal{X}$ is the shape factor. C_c is

153   the Cunningham slip correction factor for a certain diameter. Similar to other studies, the shape factor $\mathcal{X}$ is

154   assumed as 1 and C_c is neglected in the calculation (Khlystov et al., 2004; Hu et al., 2012). Therefore, the

155   electrical mobility diameter (in the range of 10.3 - 756.6 nm) was converted to the aerodynamic diameter (in

156   the range of 12.6 - 926.6 nm).

157   Taking particle mixing state into account, the particle population can be categorized into hygroscopic

158   and hydrophobic groups according to HGFs measured at RH = 98% by HH-TDMA. Particles with HGF <

159   1.2 were regarded as hydrophobic particles whereas those with HGF ≥ 1.2 were regarded as hygroscopic

160   particles (Wang et al., 2018b; Zong et al., 2021). The hydrophobic particles in urban environments have been

161   interpreted as originating from freshly emitted soot and vehicle exhaust, while the hygroscopic particles have

162   been regarded to experience long-distance transport (Swietlicki et al., 2008; Baltensperger, 2002). To obtain

163   the PNSDs for both groups, the total PNSD measured by TDMPS were scaled by the number fractions (NF)

164   of hydrophobic and hygroscopic particles. With HGF = 1.2 as the cut-off point, the GF-PDF for each selected

165   size was divided into the hydrophobic and hygroscopic modes. The calculation methods of the HGF and NF

166   of each mode were detailed in Zong et al. (2021). The NFs of size-resolved particles within the measuring

167   range of the TDMPS were calculated by linear interpolation methods, while those of particles out of the range

168   were equal to the closest known NF.

2.4 Particle Dose Estimation

170   The MPPD model (version 3.04) was used to estimate the deposition of particles in the HRT, since it

171   fits with the measured data better than the ICRP model (Londahl et al., 2007). This model calculates

172   deposition and clearance of monodisperse and polydisperse aerosols in the size range of 1 nm - 100 μm in

173   the respiratory tracts of laboratory animals, human adults, and children. Within each airway, the deposition

is calculated using theoretically derived efficiencies for deposition by diffusion, sedimentation, impaction, and interception within the airway or airway bifurcation (MPPD: Multiple-Path Particle Dosimetry Model, 2022). The model requires the following parameters as input: (1) airway morphometry parameters (airway morphometry model, functional residual capacity (FRC), and the upper respiratory tract (URT) volume); (2) particle properties (density, diameter); (3) exposure scenario (breathing frequency (BF), tidal volume (TV)); and (4) deposition/clearance.

In this study, the stochastic model (60th percentile) was chosen, which is closer to the realistic structure of human lungs (Voliotis and Samara, 2018; Li et al., 2016; Asgharian et al., 2001; Wang et al., 2021; Lyu et al., 2018; Avino et al., 2018; Manigrasso et al., 2015). The particle diameter range was set as 0.01 - 10.0 μm. Particle density was taken as 1.5 g/cm^3 according to a previous study in Beijing (Hu et al., 2012). In order to obtain the deposition pattern of different age groups, the population was divided into three groups on the basis of their age: children (7 - 12 years old), adults (18 - 26 years old), and the elderly (> 59 years old). Then, the particle deposition was estimated based on Chinese localized physiological parameters (Table 1). These values were considered for an exposure scenario for resting (e.g., sitting) and nasal breathing. All the model simulations were conducted based on this exposure scenario using the male physiological parameters, as corresponding data for females were not available. Elsewhere it was shown that males received higher doses compared to females in all age classes due to the different physiological parameters (e.g., higher TV and FRC) (Voliotis and Samara, 2018), hence similar behavior would have been expected here. It should be noticed that the exposure time data came from the statistical results of the questionnaire survey of the outdoor activity time for the rural population in Hebei, China. While, people may rest, take light exercise, or take heavy exercise during the exposure time. Different exercise levels (e.g. sitting, walking, exercising, etc) can result in different dose estimations and are not discussed here. For instance, previous studies found that the exercise level had great impact on the minute ventilation and led to the increasing deposition dose (Londahl et al., 2007). Similarly, different exposure scenarios (e.g. sleeping, exercising, walking, etc) can result in different dose estimations and are not discussed here. For instance, previous studies found that the exercise level had great impact on the minute ventilation and led to the increasing deposition dose (Londahl et al., 2007). All the other model input parameters were set as default. It should be noted that any clearance mechanisms were not considered in this study, hence our results show the upper limit of exposure.

Table 1 Physiological and breathing parameters for three age groups

Age Groups[a]	FRC/mL	Height[e]/cm	URT Volume[f]/mL	TV[e]/ mL	BF[e]/ min^{-1}	Exposure Time/ min day^{-1}
Children	1330[b,c]	139.3	21.91	630	22	96[g]
Adults	3338[d]	158.5	36.31	730	18	253[h]
Elderly	3259[d]	166.9	34.01	760	18	241[h]

[a] Base on the available data, age groups here refer to males.

[b] Due to the lack of data, the FRC value of children is not a Chinese localization parameter.

[c] Stocks and Quanjer, 1995

[d] Cao, 2009

207 [e] Zhu, 2006

208 [f] Hart et al., 1963

209 [g] Duan, 2016

210 [h] Duan et al., 2014

211 The DF is the ratio of the mass/number/surface area of the deposited particles to that of inhaled particles

212 in a given region. The DFs of hygroscopic and hydrophobic particles with considering hygroscopicity

213 (hereinafter referred to as "wet particles") were obtained based on the DFs of particles without considering

214 hygroscopicity (hereinafter referred to as "dry particles"). More specifically, it is considered that the DF of

215 wet particles with D_p after hygroscopic growth was equal to that of dry particles with the same diameter (D_p).

216 Therefore, the DF curve of wet particles corresponds to shifting the particle size range of the DF curve of dry

217 particles to the right. The daily particle number doses and deposition rates for size-resolved particles in a

218 specific region were calculated as follows (Voliotis and Samara, 2018),

$$Dose_i = DF_i \times PNC_i \times TV \times BF \times t \tag{5}$$

$$Rate_i = DF_i \times PNC_i \times TV \times BF \tag{6}$$

219 where $Dose_i$ is the deposition dose of ith size particle (#/day), $Rate_i$ is the deposition rate of ith size particle

220 (#/h), DF_i is the deposition fraction of ith size channel in a specific region, PNC_i is the particle number

221 concentration (#/cm^3) corresponding to the ith size channel, TV is the tidal volume (mL), BF is the breathing

222 frequency (min^{-1}), and t is the exposure time in ambient air (min/day). The deposition dose of a specific

223 region was calculated by adding together doses of size-resolved particles, and the total dose was the sum of

224 three regional doses. The dose without considering hygroscopicity was calculated on the basis of the dry

225 PNSD. The dose considering hygroscopicity was the sum of particle doses of hygroscopic and hydrophobic

226 groups, which was respectively calculated by the PNSD of two groups.

227 **3 Results and Discussion**

228 **3.1 Particle Number Size Distributions in the human respiratory tract**

229 As described in Sect. 2.3, particles were categorized into hygroscopic and hydrophobic groups at RH =

230 98% according to their hygroscopicity. The hygroscopicity of size-resolved particles measured by HH-

231 TDMA during the sampling period was displayed in Table S1. Figure 1 showed the average ambient PNSD

232 under dry conditions (RH < 30%) over the entire field campaign and those of hygroscopic and hydrophobic

233 particles in the HRT. The wet diameters of hydrophobic and hygroscopic particles in the HRT were shown in

234 Table S2. The average particle number concentrations (PNCs) of hygroscopic and hydrophobic particles were

235 $(1.76 \pm 1.64) \times 10^4$ (mean ± standard deviation (SD), the same below) and $(1.70 \pm 3.14) \times 10^3$ #/cm^3,

236 respectively. The hygroscopic particles accounted for an average of (91.5 ± 5.7) % of the total PNC and

237 dominated the measured aerosol population. The PNSDs of ambient aerosols during the daytime and

238 nighttime were shown in Figure S1.
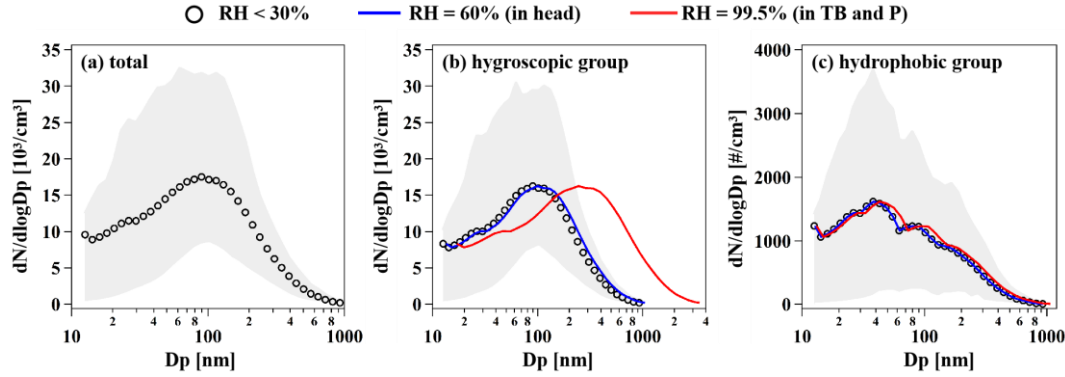
Figure 1. (a) The average particle number size distribution (PNSD) measured by TDMPS during the sampling period. The average PNSDs of the **(b)** hygroscopic and **(c)** hydrophobic groups in the human respiratory tract at different relative humidities (RHs). The black markers, blue lines, and red lines represent PNSDs under dry conditions (RH < 30%), in the head (RH = 60%), and in the TB and P (RH = 99.5%), respectively. The upper and lower edges of the grey area represent the 90th and 10th quantiles of PNSDs, respectively.

As shown in Figure 1(b), the hygroscopic particles grew slightly in the head (the blue line), while they had a remarkable growth in the TB and P regions (the red line) attributed to high humidity conditions and water uptake. Particularly, the diameter of hygroscopic particles corresponding to the maximum PNC shifted from about 90 nm to 250 nm. As expected, no obvious size growth of hydrophobic particles took place in the three regions in the HRT, and the peak appeared at $D_p \approx 40$ nm (Figure 1(c)).

3.2 Regional and Total Deposition Fractions

Taking the adults group as an example, size-resolved regional and total DFs of particles under dry conditions (black dots), and hydrophobic (blue dots) and hygroscopic (red dots) particles in humid environments were shown in Figure 2. The size-resolved DFs for the children and the elderly groups were shown in Figure S2-S3. As shown in the three figures, the regional and total DFs of all age groups respectively followed the same trends regardless the particle hygroscopicity. Due to the similar physiological parameters (such as the FRC, URT volume, TV, and BF, as shown in Table 1) of the adults (Figure 2) and the elderly (Figure S3), their regional and total DF functions were similar to each other. While, for the reason that the FRC is positively correlated with the body weight, the FRC of the children was nearly one third of those of the adults and the elderly, which may lead to the different DF curves of the children (Figure S2). Compared with the adults and the elderly, the children had lower DFs of ultrafine particles in the head and higher DFs of submicron particles in the P region, resulting in higher total DFs of submicron particles.
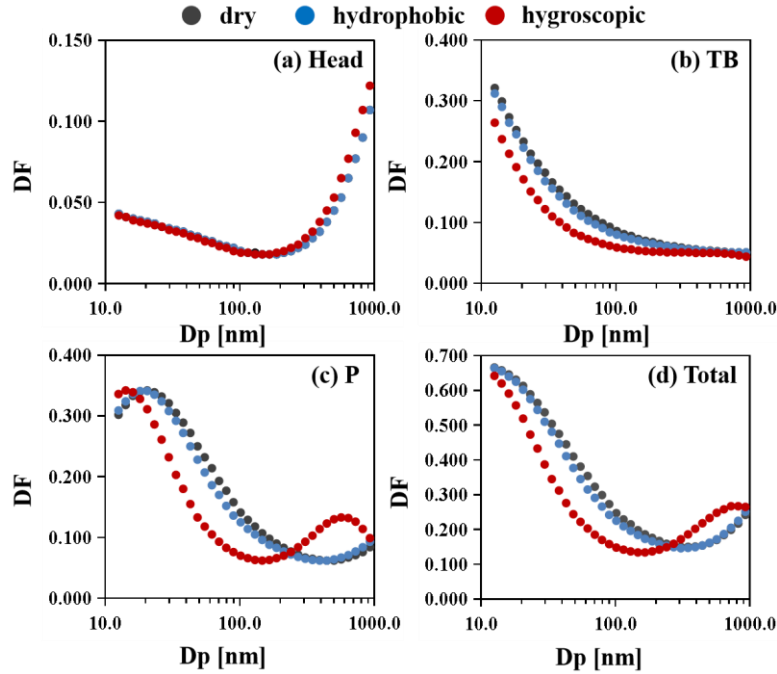
Figure 2. Size-resolved (a) head, (b) TB, (c) P, and (d) total deposition fractions (DFs) of particles under dry conditions (i.e., without considering hygroscopicity), and hydrophobic and hygroscopic particles in humid environments (i.e., considering hygroscopicity) for the adults group. For clarity, the abscissa of Figure 2 refers to the dry diameter of particles. The black, blue, and red dots represent dry, hydrophobic, and hygroscopic particles, respectively. In Figure 2(a), the black dots representing DFs under dry conditions is hidden behind the blue dots representing DFs of hydrophobic particles, because these two sets of DFs are close to each other.

As shown in Figure 2(a), there was no significant difference between head DFs whether hygroscopicity was considered or not, because the conditions within the upper respiratory tract were in balance with the surrounding environment (Ching and Kajino, 2018). With the increasing D_p, the head DFs decreased at first and reached the minimum at around 150 nm, then increased sharply, which is similar to the trend of the head DF curve using MPPD by Youn et al. (2016).

In the TB, the DF declined monotonically associated with the increasing particle diameter, and tended to plateau for particles with $D_p > \sim 100$ nm (Figure 2(b)), which is consistent with the results of previous studies (Youn et al., 2016; Hussein et al., 2019; Varghese and Gangamma, 2009). If hygroscopicity was not taken into consideration, DFs of submicron particles were overestimated for both groups (i.e., the blue dots for hydrophobic particles and the red dots for hygroscopic particles). Using the percentage of the difference between DFs in two cases (i.e., considering hygroscopicity or not) and the DF without considering hygroscopicity as a weight, tracheobronchial DFs of hydrophobic particles were overestimated by less than 9.7%, while, 23.0% on average for hygroscopic particles. For example, the DF of particles with dry diameters at around 50 nm was 0.131 without considering hygroscopicity, and it shifted to 0.120 for hydrophobic and 0.083 for hygroscopic particles considering hygroscopicity, with the differences of 8.4% and 36.6%.

Compared with size-resolved DFs of particles under dry conditions (the black dots in Figure 2(c)), the DFs of hydrophobic (the blue dots) and hygroscopic (the red dots) particles in the P region were overestimated in the range of 20 - 500 nm and 20 - 250 nm respectively, and those of particles outside the above diameter

ranges were underestimated. The DFs of hydrophobic and hygroscopic particles were respectively overestimated (underestimated) by up to 14.1% (10.7%) and 53.1% (109.7%). Similarly, taking particles with a dry particle diameter of 50 nm as an example, the DF in the P was 0.250 without considering hygroscopicity, while it reduced to 0.133 (0.228) for hygroscopic (hydrophobic) particles considering hygroscopicity. Besides, resembled with the results of Youn et al. (2016) and Varghese et al. (2009), there was only one peak at the DF curve of the P region in the submicron range without considering hygroscopicity (black dots). Considering hygroscopicity, another peak of larger hygroscopic particles ($\sim$ 800 nm) appeared. It indicates that particle hygroscopicity enables more submicron particles with relatively large diameters to deposit in the deepest parts of the lung. It should be noted that the particle density would change during hygroscopic growth, which was not considered in the calculation due to the lack of the measurement of the particle density. The sensitivity analysis of the particle density on the regional DFs was shown in Figure S4.

In Figure 2(d), the total DFs of hydrophobic particles (the blue dots) had a similar trend as those of dry particles due to regional DFs mentioned above. For the hygroscopic group (the red dots), with $D_p = 270$ nm as the boundary, DFs of smaller particles were overestimated by 27.6% on average, while those of larger particles were underestimated by 28.6% on average. When considering hygroscopicity, submicron particles undergo hygroscopic growth by water uptake, and particle sizes increase as a whole (Figure 1(b) and (c)). For small particles dominated by diffusion, as D_p increasing, Brownian motion intensity decreased, and the diffusion deposition decreased accordingly. For large particles dominated by interception and inertial impaction, these two efficiencies increased with the particle size. Therefore, the corresponding particle deposition increased. This result is consistent with the previous study using the ICRP model which concluded that the deposition of particles with $D_p < 200$ nm was overestimated without considering water uptake (Vu et al., 2015). Additionally, the trend of the total DFs in both cases in this study is similar to the experimental data of breathing NaCl with/without hygroscopicity through noses (Chalvatzaki and Lazaridis, 2018). In general, hygroscopicity has a significant effect on regional DFs of hygroscopic particles in the TB and P regions. While, no obvious variation occurred in the DFs of two groups in the head or those of hydrophodic particles in the TB and P.

3.3 Regional and Total Deposition Doses and Rates for Different Age Groups

Regional (head, TB, and P) and total deposition number doses with/without considering hygroscopicity were calculated for the children (a), adults (b), and the elderly (c) in Figure 3. Specific values of deposition doses of hydrophobic and hygroscopic particles in two cases can be found in Table S3-S5. Hussein et al. (2013) found that the deposited dose calculations in the other age groups (the elderly and teens) were in the same order of magnitudes as that of the adults. This is also true in our results. In both cases, the elderly group had the highest total deposition dose among the three groups, followed by the adults and children. While, Voliotis et al. (2018) concluded that the adults received the highest doses among all age groups, which may be caused by different physiological parameter values, such as the TV. In each group, the contribution of the P region to the total dose was the greatest ($> \sim 55\%$), which was similar to the published conclusions (Voliotis

323 and Samara, 2018; Hussein et al., 2013; Manigrasso et al., 2017; Li et al., 2016). Moreover, the proportion
324 of pulmonary deposition in total doses for the children was up to 62.9% considering hygroscopicity. By
325 comparison, it accounted for 54.6% and 55.7% for the adults and the elderly groups, respectively. This
326 indicates that particles inhaled by children are more likely to deposit in their pulmonary regions, which is in
327 accordance with the results of previous studies (Voliotis and Samara, 2018; Voliotis et al., 2021). Taking
328 hygroscopicity into consideration, total deposition doses significantly reduced by about a quarter (24.0% -
329 24.1%) for all age groups. The greatest reduction took place in doses in the P region (25.9% - 26.3%),
330 followed by doses in the TB (24.2% - 26.1%). Head deposition had only minor variations (-0.9% - +0.5%)
331 in both cases.

332
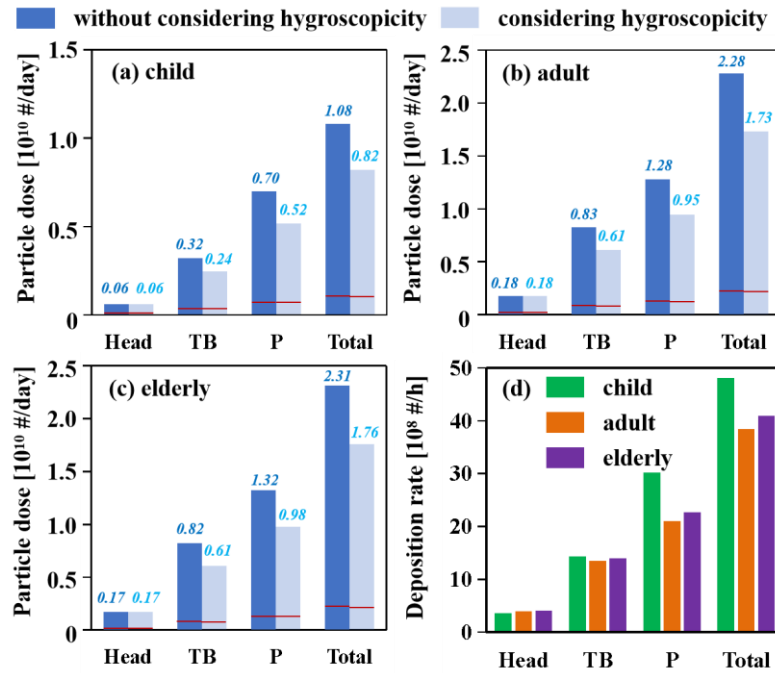
333 **Figure 3. Regional and total deposition doses for the (a) children, (b) adults, and (c) the elderly with/without**
334 **considering particle hygroscopicity. The dark blue columns represent doses without considering hygroscopicity.**
335 **The light blue columns represent doses considering hygroscopicity. The red lines on the column represent the**
336 **division of doses of hygroscopic (above the red line) and hydrophobic particles (below the red line). Numbers**
337 **above each column mean the corresponding particle doses with a unit of 10^{10} #/day. (d) The average regional and**
338 **total deposition rates considering hygroscopicity for three age groups. The green, orange, and purple column**
339 **represent the children, adults, and elderly, respectively.**

340 In both cases, the adults (Figure 3(b)) and the elderly (Figure 3(c)) groups received similar regional and
341 total doses. In contrast, the children had the minimum total dose (Figure 3(a)), which was around half (47.4%
342 on average) to that for the adults. As shown in Eq (4), the exposure time is an important parameter for
343 deposition dose calculations. The exposure time of the adults and the elderly groups was more than twice
344 than that of the children (Table 1), which resulted in the greater deposition dose for the former two groups.
345 ~~However, due to the availability of data, only localized physiological parameters for resting were obtained.~~
346 ~~People may rest, take light exercise, or take heavy exercise in the exposure time. Since the higher exercise~~
347 ~~level contributes to the greater particle deposition (Londahl et al., 2007), the actual deposition dose may be~~

348 ~~underestimated.~~ Therefore, to remove the impact of the exposure time, the regional and total deposition rates

349 for three age groups were also calculated and shown in Figure ~~S5~~3(d). The children received the maximum

350 total deposition rate ($(4.81 \pm 4.55) \times 10^9$ #/h), followed by the elderly group ($(4.09 \pm 3.92) \times 10^9$ #/h), and

351 the adults received the minimum ($(3.84 \pm 3.69) \times 10^9$ #/h). The regional deposition rate in the TB and P

352 regions for three age groups showed a same order as the total deposition rate, while the order in the head was

353 quite different. Specifically, three age groups had the similar deposition rate in the head. ~~The proportion of~~

354 ~~pulmonary deposition in total doses for children was up to 62.9% considering hygroscopicity. By comparison,~~

355 ~~it accounted for 54.6% and 55.7% for adults and the elderly groups, respectively. This indicates that particles~~

356 ~~inhaled by children are more likely to deposit in their pulmonary regions, which is in accordance with the~~

357 ~~results of previous studies (Voliotis and Samara, 2018; Voliotis et al., 2021).~~

358 As shown by the red lines in Figure 3, the contribution of hydrophobic particles to total deposition doses

359 was about 10.0% for all age groups, while it increased to 12.5% after considering hygroscopicity.

360 Hydrophobic particles were assumed to originate from freshly emitted soot and exhaust particles (Swietlicki

361 et al., 2008; Baltensperger, 2002), which are composed of species that do great harm to human health, such

362 as black carbon (BC) (Highwood and Kinnersley, 2006), primary organic aerosols (Mauderly and Chow,

363 2008), and polycyclic aromatic hydrocarbons (Kim et al., 2013; Haritash and Kaushik, 2009). Therefore, we

364 need to pay attention to the deposition effects of hydrophobic particles.

365 The adults' regional and total deposition doses of size-resolved particles with/without considering

366 hygroscopicity were shown in Figure 4. The effects of hygroscopicity in particle doses in the head (Figure

367 4(a)) are insignificant, because the RH in the upper respiratory tract was close to that under dry conditions.

368 Regional doses in the TB decreased due to particle hygroscopic growth (Figure 4(b)), and the greatest

369 reduction (~ 33%) appeared between 40 and 80 nm in diameter. Similarly, particle hygroscopicity

370 considerably decreased deposition doses (up to 50.3%) in the P region for particle sizes between 20 and 240

371 nm (Figure 4(c)). Inversely, particle doses increased (up to 102.6%) in the P region for diameters less than

372 20 nm and above 240 nm due to hygroscopic growth. As a result, the total deposition dose, as shown in Figure

373 4(d), was overestimated for particles smaller than around 270 nm with a maximum of 40.8% without

374 considering hygroscopicity. The deposition doses of particles larger than this diameter were underestimated

375 and the maximum was 43.0%.

376
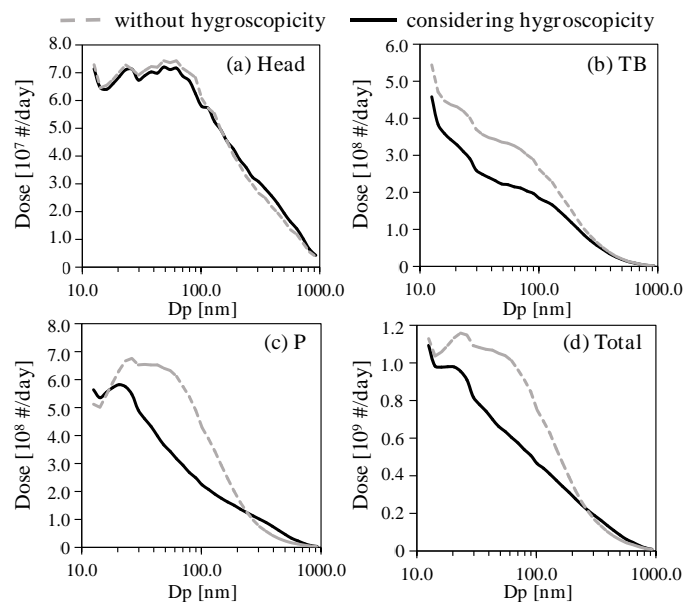
377 **Figure 4. (a) Head, (b) TB, (c) P, and (d) total deposition doses of size-resolved particles for the adults group**
378 **with/without considering hygroscopicity. For clarity, the abscissa of Figure 4 refers to the dry diameter of particles.**
379 **The grey dashed line represents doses without considering hygroscopicity. The black solid line represents doses**
380 **considering hygroscopicity.**

381 **3.4 Deposition Rates of Hygroscopic and Hydrophobic Particles**

382   In order to link human daily activities to the particulate matter deposition, the diurnal variations of

383 deposition rates of hygroscopic and hydrophobic particles considering hygroscopicity for the adults group

384 averaged over the entire field campaign were investigated and displayed in Figure 5. Additionally, the

385 average concentrations of NO, CO, BC, and OH radical were also given in Figure 5. By comparison, the

386 diurnal variations of the deposition rates of hygroscopic and hydrophobic particles without considering

387 hygroscopicity were displayed in Figure S65. No matter which time was considered during a day, the

388 deposition rate of hygroscopic particles ($(3.60 \pm 6.68) \times 10^9$ #/h) in the HRT was nearly one magnitude higher

389 than that of hydrophobic particles ($(5.15 \pm 14.4) \times 10^8$ #/h).
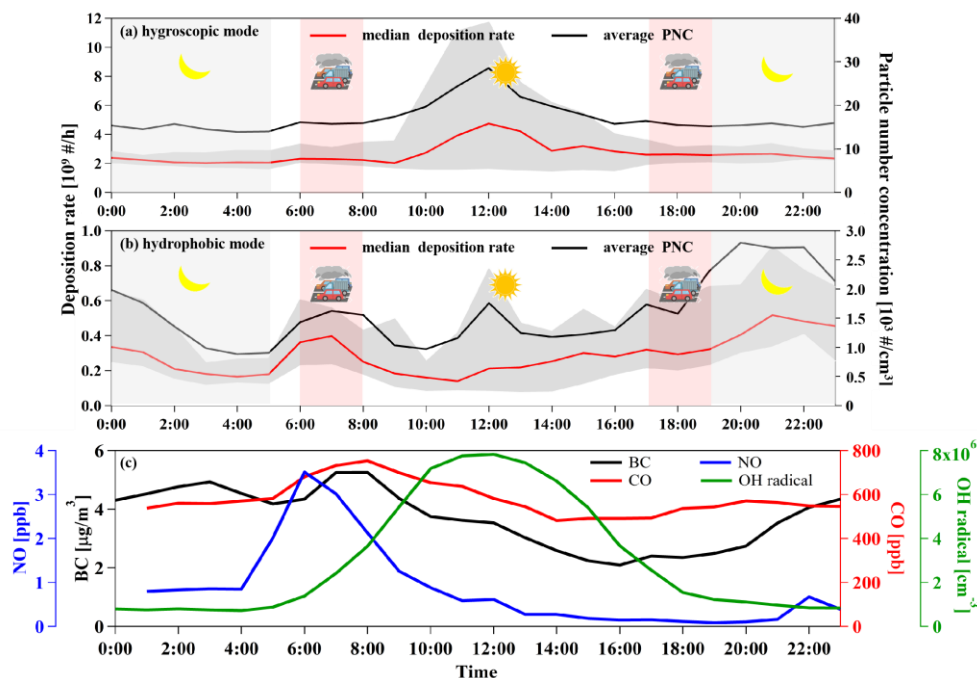
Figure 5. The diurnal variations of deposition rates considering hygroscopicity and particle number concentrations (PNCs) of (a) hygroscopic and (b) hydrophobic particles for the adults group. The red lines represent the median deposition rate. The upper and lower edges of the grey area represent the 75th and 25th quantiles of deposition rates, respectively. The black lines represent the average PNC. (c) The diurnal variations of the average concentrations of NO, CO, BC, and OH radical during the sampling period. The blue, red, black, and green lines represent NO, CO, BC, and OH radical, respectively.

The deposition rate of hygroscopic particles (Figure 5 (a)) was higher during the daytime (5:00 - 19:00, $(2.88 \times 10^9) \pm (8.10 \times 10^8)$ #/h) than that at night (from 20:00 to 4:00 the next day, $(2.32 \times 10^9) \pm (2.41 \times 10^8)$ #/h). The peak appeared at noon and the deposition rate reached the top at 12:00 (4.74×10^9 #/h on average). The enhanced deposition rate can be attributed to the strong atmospheric oxidation capacity during the daytime, indicated by OH radical in Figure 5(c), which creates new particles or transfers the pre-existing aerosols to more aged particles through nucleation, semi-volatile partitioning, and multiphase chemistry (Raes et al., 2000; Donahue et al., 2014; Tan et al., 2020; Rudich et al., 2007). For instance, a previous study pointed out that the atmospheric oxidation capacity may enhance the particle formation by oxidizing the trace gases emitted from sources (such as biomass burning) and producing low-volatility condensable vapors, which nucleates in the plume (Wu et al., 2017b). Therefore, the ultrafine particles may be produced during transport (Wu et al., 2017b). During the field campaign, the new particle formation (NPF) events took place frequently (Figure S7̶6). Our previous study showed that the NPF events and subsequent growth produced a large amount of hygroscopic and internally mixed particles (Wu et al., 2017b), thus increasing the PNC (as shown in the black line in Figure 5(a)) and leading to the enhanced deposition rate of hygroscopic particles in the day. It is indicated that the deposition rates of particles were mainly influenced by the PNC.

On the contrary, hydrophobic particles (Figure 5(b)) exhibited higher deposition rate at nighttime (($3.39 \pm 1.34) \times 10^8$ #/h) than that in the day (($2.58 \times 10^8) \pm (7.60 \times 10^7)$ #/h). The deposition rate of hydrophobic particles peaked at 6:00 - 8:00 during morning rush hours (3.37×10^8 #/h on average), as indicated by NO,

415 CO, and BC concentrations in Figure 5(c). In the evening, the deposition rate step-wisely increased and
416 reached the maximum (5.17×10^8 #/h on average) at around 21 o'clock. Correspondingly, BC concentrations
417 increased as well. The strong primary emissions (such as the biomass burning process (Wu et al., 2017a)),
418 weak chemical processes, and low boundary layer height (Zhang et al., 2014) resulted in the increased
419 hydrophobic particle number concentration. Thus, people who are exposed to outdoor air during rush hours
420 and the evening may have a higher exposure risk to hydrophobic particles.

421 ~~It is well recognized that the freshly emitted hydrophobic particles may be transferred into aged~~
422 ~~hygroscopic particles (Tan et al., 2020) via atmospheric aging with enhanced volume fractions of inorganic~~
423 ~~components and organic compounds with higher O:C (Wu et al., 2016; Jimenez et al., 2009). If we take 50~~
424 ~~nm particles as an example, the κ ranged from 0.08 to 0.46 during the entire campaign, implying their~~
425 ~~different aging degrees. Since BC primarily comes from combustion processes, the κ corresponding to the~~
426 ~~top 5% highest mass proportion of BC in the hydrophobic particles was employed to represent the κ value of~~
427 ~~primary emission particles (Figure S8). The κ of BC with D_p = 50 nm was 0.20 ± 0.12, which was lower than~~
428 ~~that of the similar size particles during the NPF events (κ = 0.37 ± 0.03) in our previous publications (Wu et~~
429 ~~al., 2017b). In this study, the total DF for adults was ~ 0.258 when κ = 0.20, while it dropped to ~ 0.217 when~~
430 ~~κ = 0.37, with a decline change of 15.9%.~~

431 **4 Conclusions and Implications**

432 To accurately quantify the effects of both hygroscopicity and external mixing state on the particle
433 deposition, the size-resolved particle hygroscopicity measured at HRT-like conditions (RH = 98%) was used
434 to estimate the deposition doses of submicron particles in the HRT for different age groups with/without
435 considering hygroscopicity using the MPPD model.

436 The total particle number concentrations were dominated by the hygroscopic particles (number fraction
437 = (91.5 ± 5.7)%). Taking hygroscopicity into consideration, total deposition doses significantly reduced by
438 about a quarter (24.0% - 24.1%) for all age groups. The greatest reduction took place in doses in the P (25.9%
439 - 26.3%) and TB (24.2% - 26.1%) regions. Head deposition had only minor variations (-0.9% - +0.5%) in
440 both cases. With 270-nm as the boundary, the total doses of smaller particles were overestimated and those
441 of larger particles were underestimated. Regardless of hygroscopicity, the elderly groups received the highest
442 total doses, and the children had the lowest doses, which was around half to that for the elderly. Pulmonary
443 doses dominated the deposition pattern. When it comes to the deposition rate, the children received the
444 maximum total deposition rate, followed by the elderly group, and the adults received the minimum. The
445 diurnal variations of deposition rates of hygroscopic and hydrophobic particles were also calculated. The
446 deposition rate of hygroscopic particles was higher during the daytime (2.88×10^9) ± (8.10×10^8 #/h vs. (2.32
447 $\times 10^9$) ± (2.41×10^8) #/h at night) attributed to the strong atmospheric oxidation capacity. Hydrophobic
448 particles exhibited higher deposition rate at nighttime (($3.39 \pm 1.34) \times 10^8$ #/h) than those in the day (($2.58 \times$
449 10^8) ± (7.60×10^7) #/h), which was associated with strong primary emissions, weak chemical processes, and
450 low boundary layer height. The traffic emissions during the rush hours also enhanced the deposition rate of

451 hydrophobic particles. ~~Additionally, fresh emitted particles have lower hygroscopicity and higher DFs~~

452 ~~compared with hygroscopic particles with the same diameter and concentration, which may result in higher~~

453 ~~deposition.~~ Based on a more explicit hygroscopicity measurement at RH = 98%, this work provides an insight

454 into the impact of hygroscopicity on the deposition pattern of submicron particles in the HRT.

455 Although the particle hygroscopicity was measured at a quite high RH (98%), there is still a gap between

456 the measurement conditions and the real HRT-conditions (RH = 99.5%). The higher RH in the lower

457 respiratory tract will lead to greater hygroscopic growth of particles. Since the particle hygroscopicity may

458 reduce the regional and total deposition doses, it is inferred that the higher RH in the lower HRT will further

459 decrease the deposition dose. Therefore, developing the advanced technology for measuring the

460 hygroscopicity in the real HRT-conditions will help to explore the influence of hygroscopicity on the particle

461 deposition in the HRT more accurately. For instance, the HH-TDMA (Suda and Petters, 2013), the Leipzig

462 Aerosol Cloud Interaction Simulator (Stratmann et al., 2004), the inverted streamwise-gradient cloud

463 condensation nuclei counter (Ruehl et al., 2010), and the filter-based differential hygroscopicity analyzer

464 (Mikhailov et al., 2011) have been used to determine the particle hygroscopicity at RHs up to 99%. In

465 particular, Mikhailov and Sergey (2020) adopted a new method with in situ restructuring to minimize the

466 influence of particle shape, and the RH was up to 99.6% with an RH measurement accuracy better than 0.4%.

467 Due to the limited measurements and physiological parameters, some vital factors which may have

468 effect on the particle deposition in the HRT were not considered in this study, such as gender, the exercise

469 level, and the particle density. Besides, the deposition pattern of particles with diameters larger than 1 μm

470 was not discussed here due to the lack of the measurement of the PNSD and hygroscopicity of coarse particles.

471 While, as an important part of the ambient particle mass, coarse particles may also make a significant

472 contribution to the particle deposition in the HRT (Figure S7~~9~~). The related research to find out the impact

473 of the particle hygroscopicity on the deposition mass dose of coarse particles ought to be carried out in the

474 future.

475

476 *Data availability.* The data presented in this article can be accessed on the open accessible research data

477 repository.

478 *Author contribution.* ZW, JG, DP, LZ, HH, and AW carried out the field observation and obtained data. RM,

479 ~~and~~ TZ, and YQ processed and analyzed data. All authors discussed the results and contributed to the writing

480 of this paper. RM prepared the manuscript with the contributions of all co-authors. ZW, AV, and MH further

481 modified and improved the manuscript.

482 *Competing interests.* The authors declare that they have no conflict of interest.

483 *Acknowledgements.* We gratefully acknowledge Applied Research Associates, Inc. (ARA), The Hamner

484 Institutes for Health Sciences, the National Institute of Public Health and the Environment (RIVM), and the

485 Ministry of Housing, Spatial Planning and the Environment for developing and freely distributing the MPPD

486 software.

487 *Financial support.* This work was supported by National Natural Science Foundation of China (NSFC, grant

488   no. 42011530121, 91844301) .

References

Asgharian, B., Hofmann, W., and Bergmann, R.: Particle Deposition in a Multiple-Path Model of the Human Lung, Aerosol Sci. Technol., 34, 332-339, 10.1080/02786820119122, 2001.

Avino, P., Scungio, M., Stabile, L., Cortellessa, G., Buonanno, G., and Manigrasso, M.: Second-hand aerosol from tobacco and electronic cigarettes: Evaluation of the smoker emission rates and doses and lung cancer risk of passive smokers and vapers, Sci. Total Environ., 642, 137-147, 10.1016/j.scitotenv.2018.06.059, 2018.

Baltensperger, U.: Urban and rural aerosol characterization of summer smog events during the PIPAPO field campaign in Milan, Italy, J. Geophys. Res., 107, 10.1029/2001jd001292, 2002.

Bian, Y. X., Zhao, C. S., Ma, N., Chen, J., and Xu, W. Y.: A study of aerosol liquid water content based on hygroscopicity measurements at high relative humidity in the North China Plain, Atmos. Chem. Phys., 14, 6417-6426, 10.5194/acp-14-6417-2014, 2014.

Birmili, W., Stratmann, F., and Wiedensohler, A.: Design of a DMA-based size spectrometer for a large particle size range and stable operation, J. Aerosol Sci., 30, 549-553, 10.1016/S0021-8502(98)00047-0, 1999.

Cao, L.: The geographical distribution of normal reference value of lung compliance and total lung capacity. Shaanxi Normal University, Xi'an, Shaanxi, China, 2009.

Chalvatzaki, E. and Lazaridis, M.: A dosimetry model of hygroscopic particle growth in the human respiratory tract, Air Qual., Atmos. Health, 11, 471-482, 10.1007/s11869-018-0555-7, 2018.

Chen, S., Wang, H., Lu, K., Zeng, L., Hu, M., and Zhang, Y.: The trend of surface ozone in Beijing from 2013 to 2019: Indications of the persisting strong atmospheric oxidation capacity, Atmos. Environ., 242, 10.1016/j.atmosenv.2020.117801, 2020.

Chen, Y., Ebenstein, A., Greenstone, M., and Li, H.: Evidence on the impact of sustained exposure to air pollution on life expectancy from China's Huai River policy, Proc. Natl. Acad. Sci. U. S. A., 110, 12936-12941, 10.1073/pnas.1300018110, 2013.

Ching, J. and Kajino, M.: Aerosol mixing state matters for particles deposition in human respiratory system, Sci. Rep., 8, 8864, 10.1038/s41598-018-27156-z, 2018.

Correia, A. W., Pope, C. A., 3rd, Dockery, D. W., Wang, Y., Ezzati, M., and Dominici, F.: Effect of air pollution control on life expectancy in the United States: an analysis of 545 U.S. counties for the period from 2000 to 2007, Epidemiology, 24, 23-31, 10.1097/EDE.0b013e3182770237, 2013.

Duan, X.: Highlights of the Chinese Exposure Factors Handbook (children), China Environment Publishing Group, Beijing, China, 2016.

Duan, X., Zhao, X., Wang, B., Chen, Y., Cao S.: Highlights of the Chinese Exposure Factors Handbook (Adults), Science Press, Beijing, China, 2014.

Dockery, D. W., Pope, C. A., 3rd, Xu, X., Spengler, J. D., Ware, J. H., Fay, M. E., Ferris, B. G., Jr., and Speizer, F. E.: An association between air pollution and mortality in six U.S. cities, N. Engl. J. Med., 329, 1753-1759, 10.1056/nejm199312093292401, 1993.

Donahue, N. M., Robinson, A. L., Trump, E. R., Riipinen, I., and Kroll, J. H.: Volatility and aging of atmospheric organic aerosol, Top. Curr. Chem., 339, 97-143, 10.1007/128_2012_355, 2014.

Farkas, A., Furi, P., Then, W., and Salma, I.: Effects of hygroscopic growth of ambient urban aerosol particles on their modelled regional and local deposition in healthy and COPD-compromised human respiratory system, Sci. Total Environ., 806, 10.1016/j.scitotenv.2021.151202, 2022.

Ferron, G. A.: The size of soluble aerosol particles as a function of the humidity of the air. Application to the human respiratory tract, J. Aerosol Sci., 8, 251-267, https://doi.org/10.1016/0021-8502(77)90045-3, 1977.

Gysel, M., McFiggans, G. B., and Coe, H.: Inversion of tandem differential mobility analyser (TDMA) measurements, J. Aerosol Sci., 40, 134-151, 10.1016/j.jaerosci.2008.07.013, 2009.

Haddrell, A. E., Davies, J. F., and Reid, J. P.: Dynamics of Particle Size on Inhalation of Environmental Aerosol and Impact on Deposition Fraction, Environ. Sci. Technol., 49, 14512-14521, 10.1021/acs.est.5b01930, 2015.

Haritash, A. K. and Kaushik, C. P.: Biodegradation aspects of polycyclic aromatic hydrocarbons (PAHs): a review, J. Hazard. Mater., 169, 1-15, 10.1016/j.jhazmat.2009.03.137, 2009.

Hart, M. C., Cook, C. D., and Orzalesi, M. M.: RELATION BETWEEN ANATOMIC RESPIRATORY DEAD SPACE AND BODY SIZE AND LUNG VOLUME, J. Appl. Physiol., 18, 519-&,

543   10.1152/jappl.1963.18.3.519, 1963.

544 Hennig, T., Massling, A., Brechtel, F. J., and Wiedensohler, A.: A Tandem DMA for highly temperature-
545   stabilized hygroscopic particle growth measurements between 90% and 98% relative humidity, J.
546   Aerosol Sci., 36, 1210-1223, 10.1016/j.jaerosci.2005.01.005, 2005.

547 Highwood, E. J. and Kinnersley, R. P.: When smoke gets in our eyes: the multiple impacts of atmospheric
548   black carbon on climate, air quality and health, Environ. Int., 32, 560-566, 10.1016/j.envint.2005.12.003,
549   2006.

550 Hofmann, W.: Modelling inhaled particle deposition in the human lung—A review, J. Aerosol Sci., 42, 693-
551   724, 10.1016/j.jaerosci.2011.05.007, 2011.

552 Hu, M., Peng, J., Sun, K., Yue, D., Guo, S., Wiedensohler, A., and Wu, Z.: Estimation of size-resolved
553   ambient particle density based on the measurement of aerosol number, mass, and chemical size
554   distributions in the winter in Beijing, Environ. Sci. Technol., 46, 9941-9947, 10.1021/es204073t, 2012.

555 Hussein, T., Saleh, S., dos Santos, V., Boor, B., Koivisto, A., and Löndahl, J.: Regional Inhaled Deposited
556   Dose of Urban Aerosols in an Eastern Mediterranean City, Atmosphere, 10, 10.3390/atmos10090530,
557   2019.

558 Hussein, T., Londahl, J., Paasonen, P., Koivisto, A. J., Petaja, T., Hameri, K., and Kulmala, M.: Modeling
559   regional deposited dose of submicron aerosol particles, Sci. Total Environ., 458-460, 140-149,
560   10.1016/j.scitotenv.2013.04.022, 2013.

561 ICRP (1994) Human respiratory tract model for radiological protection.

562 Jimenez, J. L., Canagaratna, M. R., Donahue, N. M., Prevot, A. S. H., Zhang, Q., Kroll, J. H., DeCarlo, P. F.,
563   Allan, J. D., Coe, H., Ng, N. L., Aiken, A. C., Docherty, K. S., Ulbrich, I. M., Grieshop, A. P., Robinson,
564   A. L., Duplissy, J., Smith, J. D., Wilson, K. R., Lanz, V. A., Hueglin, C., Sun, Y. L., Tian, J., Laaksonen,
565   A., Raatikainen, T., Rautiainen, J., Vaattovaara, P., Ehn, M., Kulmala, M., Tomlinson, J. M., Collins, D.
566   R., Cubison, M. J., Dunlea, E. J., Huffman, J. A., Onasch, T. B., Alfarra, M. R., Williams, P. I., Bower,
567   K., Kondo, Y., Schneider, J., Drewnick, F., Borrmann, S., Weimer, S., Demerjian, K., Salcedo, D.,
568   Cottrell, L., Griffin, R., Takami, A., Miyoshi, T., Hatakeyama, S., Shimono, A., Sun, J. Y., Zhang, Y. M.,
569   Dzepina, K., Kimmel, J. R., Sueper, D., Jayne, J. T., Herndon, S. C., Trimborn, A. M., Williams, L. R.,
570   Wood, E. C., Middlebrook, A. M., Kolb, C. E., Baltensperger, U., and Worsnop, D. R.: Evolution of
571   Organic Aerosols in the Atmosphere, Science, 326, 1525-1529, 10.1126/science.1180353, 2009.

572 Khlystov, A., Stanier, C., and Pandis, S. N.: An Algorithm for Combining Electrical Mobility and
573   Aerodynamic Size Distributions Data when Measuring Ambient Aerosol Special Issue ofAerosol
574   Science and Technologyon Findings from the Fine Particulate Matter Supersites Program, Aerosol Sci.
575   Technol., 38, 229-238, 10.1080/02786820390229543, 2004.

576 Kim, K. H., Jahan, S. A., Kabir, E., and Brown, R. J.: A review of airborne polycyclic aromatic hydrocarbons
577   (PAHs) and their human health effects, Environ. Int., 60, 71-80, 10.1016/j.envint.2013.07.019, 2013.

578 Li, X., Yan, C., Patterson, R. F., Zhu, Y., Yao, X., Zhu, Y., Ma, S., Qiu, X., Zhu, T., and Zheng, M.: Modeled
579   deposition of fine particles in human airway in Beijing, China, Atmos. Environ., 124, 387-395,
580   10.1016/j.atmosenv.2015.06.045, 2016.

581 Liu, P., Song, M., Zhao, T., Gunthe, S. S., Ham, S., He, Y., Qin, Y. M., Gong, Z., Amorim, J. C., Bertram, A.
582   K., and Martin, S. T.: Resolving the mechanisms of hygroscopic growth and cloud condensation nuclei
583   activity for organic particulate matter, Nat. Commun., 9, 4076, 10.1038/s41467-018-06622-2, 2018.

584 Londahl, J., Massling, A., Pagels, J., Swietlicki, E., Vaclavik, E., and Loft, S.: Size-resolved respiratory-tract
585   deposition of fine and ultrafine hydrophobic and hygroscopic aerosol particles during rest and exercise,
586   Inhal. Toxicol., 19, 109-116, 10.1080/08958370601051677, 2007.

587 Lyu, Y., Guo, H., Cheng, T., and Li, X.: Particle Size Distributions of Oxidative Potential of Lung-Deposited
588   Particles: Assessing Contributions from Quinones and Water-Soluble Metals, Environ. Sci. Technol., 52,
589   6592-6600, 10.1021/acs.est.7b06686, 2018.

590 Manigrasso, M., Vernale, C., and Avino, P.: Traffic aerosol lobar doses deposited in the human respiratory
591   system, Environ. Sci. Pollut. Res. Int., 24, 13866-13873, 10.1007/s11356-015-5666-1, 2017.

592 Manigrasso, M., Buonanno, G., Fuoco, F. C., Stabile, L., and Avino, P.: Aerosol deposition doses in the human
593   respiratory tree of electronic cigarette smokers, Environ. Pollut., 196, 257-267,
594   10.1016/j.envpol.2014.10.013, 2015.

595 Mauderly, J. L. and Chow, J. C.: Health effects of organic aerosols, Inhal. Toxicol., 20, 257-288,
596   10.1080/08958370701866008, 2008.

597 Mikhailov, E. F., Merkulov, V. V., Vlasenko, S. S., Ryshkevich, T. I., and Poschl, U. J.: Filter-based
598   differential hygroscopicity analyzer of aerosol particles, Izv. Atmos. Ocean. Phy., 47, 747-759,

599   10.1134/s0001433811060107, 2011.

600 Mikhailov, E. F. and Vlasenko, S. S.: High-humidity tandem differential mobility analyzer for accurate
601   determination of aerosol hygroscopic growth, microstructure, and activity coefficients over a wide range
602   of relative humidity, Atmos. Meas. Tech., 13, 2035-2056, 10.5194/amt-13-2035-2020, 2020.

603 Mitsakou, C., Housiadas, C., Eleftheriadis, K., Vratolis, S., Helmis, C., and Asimakopoulos, D.: Lung
604   deposition of fine and ultrafine particles outdoors and indoors during a cooking event and a no activity
605   period, Indoor Air, 17, 143-152, 10.1111/j.1600-0668.2006.00464.x, 2007.

606 MPPD: Multiple-Path Particle Dosimetry Model: https://www.ara.com/mppd/, last access: 2022.

607 Oberdorster, G.: Pulmonary effects of inhaled ultrafine particles, Int. Arch. Occup. Environ. Health, 74, 1-8,
608   2001.

609 Petters, M. D. and Kreidenweis, S. M.: A single parameter representation of hygroscopic growth and cloud
610   condensation nucleus activity, Atmos. Chem. Phys., 7, 1961-1971, 10.5194/acp-7-1961-2007, 2007.

611 Pope, C. A., 3rd and Dockery, D. W.: Air pollution and life expectancy in China and beyond, Proc. Natl. Acad.
612   Sci. U. S. A., 110, 12861-12862, 10.1073/pnas.1310925110, 2013.

613 Pope, C. A., III, Ezzati, M., and Dockery, D. W.: Fine-Particulate Air Pollution and Life Expectancy in the
614   United States, N. Engl. J. Med., 360, 376-386, 10.1056/NEJMsa0805646, 2009.

615 Raes, F., Dingenen, R. V., Vignati, E., Wilson, J., Putaud, J.-P., Seinfeld, J. H., and Adams, P.: Formation and
616   cycling of aerosols in the global troposphere, Atmos. Environ., 34, 4215-4240,
617   https://doi.org/10.1016/S1352-2310(00)00239-9, 2000.

618 Rudich, Y., Donahue, N. M., and Mentel, T. F.: Aging of organic aerosol: bridging the gap between laboratory
619   and field studies, Annu. Rev. Phys. Chem., 58, 321-352, 10.1146/annurev.physchem.58.032806.104432,
620   2007.

621 Ruehl, C. R., Chuang, P. Y., and Nenes, A.: Aerosol hygroscopicity at high (99 to 100%) relative humidities,
622   Atmos. Chem. Phys., 10, 1329-1344, 10.5194/acp-10-1329-2010, 2010.

623 Stocks, J. and Quanjer, P. H.: Reference values for residual volume, functional residual capacity and total
624   lung capacity. ATS Workshop on Lung Volume Measurements. Official Statement of The European
625   Respiratory Society, Eur. Respir. J., 8, 492-506, 10.1183/09031936.95.08030492, 1995.

626 Stratmann, F., Kiselev, A., Wurzler, S., Wendisch, M., Heintzenberg, J., Charlson, R. J., Diehl, K., Wex, H.,
627   and Schmidt, S.: Laboratory studies and numerical simulations of cloud droplet formation under realistic
628   supersaturation conditions, J. Atmos. Ocean. Tech., 21, 876-887, 10.1175/1520-
629   0426(2004)021<0876:Lsanso>2.0.Co;2, 2004.

630 Suda, S. R. and Petters, M. D.: Accurate Determination of Aerosol Activity Coefficients at Relative
631   Humidities up to 99% Using the Hygroscopicity Tandem Differential Mobility Analyzer Technique,
632   Aerosol Sci. Tech., 47, 991-1000, 10.1080/02786826.2013.807906, 2013.

633 Swietlicki, E., Hansson, H. C., Hameri, K., Svenningsson, B., Massling, A., McFiggans, G., McMurry, P. H.,
634   Petaja, T., Tunved, P., Gysel, M., Topping, D., Weingartner, E., Baltensperger, U., Rissler, J.,
635   Wiedensohler, A., and Kulmala, M.: Hygroscopic properties of submicrometer atmospheric aerosol
636   particles measured with H-TDMA instruments in various environments - a review, Tellus B, 60, 432-
637   469, 10.1111/j.1600-0889.2008.00350.x, 2008.

638 Tan, T., Guo, S., Wu, Z., He, L., Huang, X., and Hu, M.: Impact of aging process on atmospheric black carbon
639   aerosol properties and climate effects, Chin. Sci. Bull., 65, 4235-4250, 10.1360/tb-2020-0745, 2020.

640 Tan, Z., Hofzumahaus, A., Lu, K., Brown, S. S., Holland, F., Huey, L. G., Kiendler-Scharr, A., Li, X., Liu,
641   X., Ma, N., Min, K. E., Rohrer, F., Shao, M., Wahner, A., Wang, Y., Wiedensohler, A., Wu, Y., Wu, Z.,
642   Zeng, L., Zhang, Y., and Fuchs, H.: No Evidence for a Significant Impact of Heterogeneous Chemistry
643   on Radical Concentrations in the North China Plain in Summer 2014, Environ. Sci. Technol., 54, 5973-
644   5979, 10.1021/acs.est.0c00525, 2020.

645 Topping, D. O. and McFiggans, G.: Tight coupling of particle size, number and composition in atmospheric
646   cloud droplet activation, Atmos. Chem. Phys., 12, 3253-3260, 10.5194/acp-12-3253-2012, 2012.

647 Varghese, S. K. and Gangamma, S.: Particle deposition in human respiratory system: deposition of
648   concentrated hygroscopic aerosols, Inhal. Toxicol., 21, 619-630, 10.1080/08958370802380792, 2009.

649 Voliotis, A. and Samara, C.: Submicron particle number doses in the human respiratory tract: implications
650   for urban traffic and background environments, Environ. Sci. Pollut. Res. Int., 25, 33724-33735,
651   10.1007/s11356-018-3253-y, 2018.

652 Voliotis, A., Bezantakos, S., Besis, A., Shao, Y., and Samara, C.: Mass dose rates of particle-bound organic
653   pollutants in the human respiratory tract: Implications for inhalation exposure and risk estimations, Int.
654   J. Hyg. Environ. Health, 234, 113710, 10.1016/j.ijheh.2021.113710, 2021.

Vu, T., Delgado-Saborit, J., and Harrison, R.: A review of hygroscopic growth factors of submicron aerosols from different sources and its implication for calculation of lung deposition efficiency of ambient aerosols, Air Qual., Atmos. Health, 8, 429-440, 10.1007/s11869-015-0365-0, 2015.

Vu, T. V., Zauli-Sajani, S., Poluzzi, V., and Harrison, R. M.: Factors controlling the lung dose of road traffic-generated sub-micrometre aerosols from outdoor to indoor environments, Air Qual., Atmos. Health, 11, 615-625, 10.1007/s11869-018-0568-2, 2018.

Wang, H., Yin, P., Fan, W., Wang, Y., Dong, Z., Deng, Q., and Zhou, M.: Mortality Risk Associated with Short-Term Exposure to Particulate Matter in China: Estimating Error and Implication, Environ. Sci. Technol., 55, 1110-1121, 10.1021/acs.est.0c05095, 2021.

Wang, L., Zheng, X., Stevanovic, S., Wu, X., Xiang, Z., Yu, M., and Liu, J.: Characterization particulate matter from several Chinese cooking dishes and implications in health effects, J. Environ. Sci. (China), 72, 98-106, 10.1016/j.jes.2017.12.015, 2018a.

Wang, T., Du, Z., Tan, T., Xu, N., Hu, M., Hu, J., and Guo, S.: Measurement of aerosol optical properties and their potential source origin in urban Beijing from 2013-2017, Atmos. Environ., 206, 293-302, 10.1016/j.atmosenv.2019.02.049, 2019.

Wang, X., Shen, X. J., Sun, J. Y., Zhang, X. Y., Wang, Y. Q., Zhang, Y. M., Wang, P., Xia, C., Qi, X. F., and Zhong, J. T.: Size-resolved hygroscopic behavior of atmospheric aerosols during heavy aerosol pollution episodes in Beijing in December 2016, Atmos. Environ., 194, 188-197, 10.1016/j.atmosenv.2018.09.041, 2018b.

Wex, H., Petters, M. D., Carrico, C. M., Hallbauer, E., Massling, A., McMeeking, G. R., Poulain, L., Wu, Z., Kreidenweis, S. M., and Stratmann, F.: Towards closing the gap between hygroscopic growth and activation for secondary organic aerosol: Part 1 – Evidence from measurements, Atmos. Chem. Phys., 9, 3987-3997, 10.5194/acp-9-3987-2009, 2009.

Wiedensohler, A., Birmili, W., Nowak, A., Sonntag, A., Weinhold, K., Merkel, M., Wehner, B., Tuch, T., Pfeifer, S., Fiebig, M., Fjäraa, A. M., Asmi, E., Sellegri, K., Depuy, R., Venzac, H., Villani, P., Laj, P., Aalto, P., Ogren, J. A., Swietlicki, E., Williams, P., Roldin, P., Quincey, P., Hüglin, C., Fierz-Schmidhauser, R., Gysel, M., Weingartner, E., Riccobono, F., Santos, S., Grüning, C., Faloon, K., Beddows, D., Harrison, R., Monahan, C., Jennings, S. G., O'Dowd, C. D., Marinoni, A., Horn, H. G., Keck, L., Jiang, J., Scheckman, J., McMurry, P. H., Deng, Z., Zhao, C. S., Moerman, M., Henzing, B., de Leeuw, G., Löschau, G., and Bastian, S.: Mobility particle size spectrometers: harmonization of technical standards and data structure to facilitate high quality long-term observations of atmospheric particle number size distributions, Atmos. Meas. Tech., 5, 657-685, 10.5194/amt-5-657-2012, 2012.

Wu, Z., Zheng, J., Wang, Y., Shang, D., Du, Z., Zhang, Y., and Hu, M.: Chemical and physical properties of biomass burning aerosols and their CCN activity: A case study in Beijing, China, Sci. Total Environ., 579, 1260-1268, 10.1016/j.scitotenv.2016.11.112, 2017a.

Wu, Z. J., Zheng, J., Shang, D. J., Du, Z. F., Wu, Y. S., Zeng, L. M., Wiedensohler, A., and Hu, M.: Particle hygroscopicity and its link to chemical composition in the urban atmosphere of Beijing, China, during summertime, Atmos. Chem. Phys., 16, 1123-1138, 10.5194/acp-16-1123-2016, 2016.

Wu, Z. J., Ma, N., Größ, J., Kecorius, S., Lu, K. D., Shang, D. J., Wang, Y., Wu, Y. S., Zeng, L. M., Hu, M., Wiedensohler, A., and Zhang, Y. H.: Thermodynamic properties of nanoparticles during new particle formation events in the atmosphere of North China Plain, Atmos. Res., 188, 55-63, 10.1016/j.atmosres.2017.01.007, 2017b.

Wu, Z. J., Poulain, L., Henning, S., Dieckmann, K., Birmili, W., Merkel, M., van Pinxteren, D., Spindler, G., Müller, K., Stratmann, F., Herrmann, H., and Wiedensohler, A.: Relating particle hygroscopicity and CCN activity to chemical composition during the HCCT-2010 field campaign, Atmos. Chem. Phys., 13, 7983-7996, 10.5194/acp-13-7983-2013, 2013.

Youn, J. S., Csavina, J., Rine, K. P., Shingler, T., Taylor, M. P., Saez, A. E., Betterton, E. A., and Sorooshian, A.: Hygroscopic Properties and Respiratory System Deposition Behavior of Particulate Matter Emitted by Mining and Smelting Operations, Environ. Sci. Technol., 50, 11706-11713, 10.1021/acs.est.6b03621, 2016.

Zhang, Y., Zhang, S., Huang, C., Huang, K., Gong, Y., and Gan, Q.: Diurnal variations of the planetary boundary layer height estimated from intensive radiosonde observations over Yichang, China, Sci. China: Technol. Sci., 57, 2172-2176, 10.1007/s11431-014-5639-5, 2014.

Zong, T., Wang, H., Wu, Z., Lu, K., Wang, Y., Zhu, Y., Shang, D., Fang, X., Huang, X., He, L., Ma, N., Gross, J., Huang, S., Guo, S., Zeng, L., Herrmann, H., Wiedensohler, A., Zhang, Y., and Hu, M.: Particle hygroscopicity inhomogeneity and its impact on reactive uptake, Sci. Total Environ., 151364,

711   10.1016/j.scitotenv.2021.151364, 2021.

712   Zhu, G.: Physiological constants and psychological status of Chinese population, Peking Union Medical
713   College, Beijing, China, 2006.